Oxidative Degradation of Dihydrofolate Reductase Increases CD38-Mediated Ferroptosis Susceptibility

Yingying Ma
Tsinghua University
Meiqi Yi
BeiGene (Beijing) Co., Ltd.
Weixuan Wang
Guangdong Pharmaceutical University https://orcid.org/0000-0002-2613-589X
Liu Xiaohui
Tsinghua university
Qingtao Wang
Beijing Chaoyang Hospital affiliated Capital Medical University
Chongdong Liu
Chao Yang Hospital of Capital Medical University
Yuling Chen
Tsinghua University
Haiteng Deng (dht@mail.tsinghua.edu.cn)
Tsinghua University https://orcid.org/0000-0001-9496-1280

Article

Keywords:

Posted Date: July 1st, 2022

DOI: https://doi.org/10.21203/rs.3.rs-1725582/v1

Version of Record: A version of this preprint was published at Cell Death & Disease on November 9th, 2022. See the published version at https://doi.org/10.1038/s41419-022-05383-7.

Abstract

High expression of CD38 in tissues is a characteristic of aging, resulting in a decline in nicotinamide adenine dinucleotide (NAD) and increasing cellular reactive oxygen species (ROS). However, whether CD38 increases susceptibility to ferroptosis remains largely unexplored. Our previous study showed that CD38 overexpression decreased dihydrofolate reductase (DHFR). In the present study, we confirmed that high expression of CD38 increased ROS levels and induced DHFR degradation, which was prevented by nicotinamide mononucleotide (NMN) replenishment. We further revealed that ROS-mediated sulfonation on Cys7 of DHFR induced its degradation via the proteasome pathway while C7A mutation abolished ROS-induced DHFR degradation. Moreover, oxidative degradation of DHFR was responsible for the increased ferroptosis susceptibility in cells in which CD38 was highly expressed. We also found that CD38 expression was higher in bone-marrow derived macrophages (BMDMs) from aged mice than that from young mice, while DHFR level was lower. Consequently, we demonstrated that BMDMs from aged mice were more susceptible to ferroptosis that can be reverted by NMN replenishment, suggesting that CD38 high expression rendered cells more susceptible to ferroptosis. Taken together, these results indicated that CD38-mediated NAD^+ decline promoted DHFR oxidative degradation, thus resulting in increased cellular susceptibility to ferroptosis and suggested that NMN replenishment may protect macrophages from ferroptosis in aged mice.

Introduction

Nicotinamide adenine dinucleotide (NAD), found in all living cells, is involved in the redox reactions and various biological processes such as circadian rhythm and inflammation. As an essential co-factor of redox enzymes and a substrate for deacetylases, NAD^+ decline during chronological aging results in mitochondrial dysfunction, oxidative stress, DNA damage, and cognitive impairment (1, 2). As the main NAD^+-degrading enzyme in mammalian tissues, CD38 mainly catalyzes NAD^+ to adenosine diphosphate ribose (ADPR) and to a lesser extent to cyclic adenosine diphosphate ribose (cADPR) (3). The expression level and activity of CD38 has been shown to increase with age in various tissues and macrophages, thus resulting in age-related NAD^+ decline. Consequently, CD38 inhibition or knockout has been proven to preserve NAD^+ levels in tissues during aging and to increase lifespan, healthspan, and glucose tolerance (4–6). Replenishment of NAD^+ precursors including nicotinamide mononucleotide (NMN), nicotinamide riboside (NR), nicotinamide (NAM), niacin (NA) or inhibition of NAD^+-consuming enzymes has also been shown to prolong healthspan and to treat age-related disorders (ARDs) (7, 8).

Ferroptosis is a new form of regulated cell death different from apoptosis, autophagy, and necrosis and is characterized by iron-dependent lipid peroxidation (9, 10). The direct cause of ferroptosis is the lipid peroxides produced by the reaction of polyunsaturated fatty acids (PUFAs) of the membrane and hydroxyl radical, which is the product of Fenton reaction catalyzed by ferrous ion (11, 12). The mechanism of ferroptosis is mainly grouped into five aspects i.e., (i) inhibition of cysteine/glutamate antiporter (System X_C^-), (ii) depletion of glutathione or inhibition of phospholipid hydroperoxide

glutathione peroxidase 4 (GPX4), (iii) excessive iron accumulation, especially ferrous ion, (iv) the decrease of lipid peroxide reducers including tetrahydrobiopterin (BH_4), coenzyme Q10 (CoQ_{10}), and (v) excessive accumulation of lipid peroxides (13–15). In addition, ferroptosis has been reported to play a pivotal role in aging and diverse diseases such as aging-related neurodegenerative disorders, cancers, and ischemia-reperfusion due to the iron accumulation and increased oxidative stress (16–18).

CD38 high expression aggravated cellular ROS levels, which may increase the susceptibility to ferroptosis. However, few studies have been reported on the relationship between CD38 expression and ferroptosis. Our previous results have shown that NAD^+ decline caused by CD38 high expression triggered ROS-mediated degradation of 15-hydroxyprostaglandin dehydrogenase (15-PGDH) to promote epithelial-mesenchymal transition (EMT). We also noticed that the level of dihydrofolate reductase (DHFR) was significantly decreased in CD38-overexpression cells from proteomic analysis (19). As a newly discovered negative regulator of ferroptosis, DHFR catalyzes the reduction of dihydrobiopterin (BH_2) to BH_4, which specifically reduces lipid peroxides thus inhibiting ferroptosis or alleviating cellular susceptibility to ferroptosis (20, 21). Therefore, we proposed that CD38 overexpression increased the susceptibility to ferroptosis by causing oxidative degradation of DHFR.

In the present study, we established a cell line in which CD38 was overexpressed and we demonstrated that high expression of CD38 increased cellular ROS levels and increased ferroptosis susceptibility. On the other hand, NMN supplementation prevented the oxidative degradation of DHFR that decreased ferroptosis susceptibility. We further showed that the bone-marrow derived macrophages (BMDMs) from aged mice had the higher CD38 expression than those from young mice, rendering them more susceptible to ferroptosis. Taken together, our work established a new link between high expression of CD38 and ferroptosis.

Results

CD38 high expression induces the oxidative degradation of DHFR

We established a cell model to mimic decreased NAD^+ levels during aging by overexpressing N-terminal truncated CD38 in A549 cells (A549-CD38) as previously reported (19). The CD38 overexpression was confirmed by western blotting (Fig. 1A). ROS levels were significantly elevated in A549-CD38 cells (Fig. 1B) while cellular NAD^+ and $NADP^+$ levels were reduced by about 55% determined by the metabolomics analysis (Fig. 1C and D). According to the proteomic results published previously (19), we noticed that the protein level of DHFR was significantly reduced in A549-CD38 cells compared with A549-Plvx cells, which was further confirmed via western blotting (Fig. 1E). However, we found that *DHFR* mRNA was slightly increased in A549-CD38 cells (Fig. 1F), suggesting that DHFR decrease was due to its degradation. To further confirm whether NAD^+ reduction was responsible for a decrease in DHFR, we treated A549-CD38 cells with FK866, an inhibitor of nicotinamide phosphoribosyltransferase (NAMPT).

Our results demonstrated that FK866 treatment also caused the decline in DHFR protein level but its mRNA level wasn't decreased (Fig. 1G and H), which implied the reduction of DHFR protein levels was partly caused by decreasing NAD^+.

NAD^+ precursors, NMN, NAM, NR, and NA, have been shown to boost intracellular NAD^+ levels (22–24). To explore whether NMN has an effect on DHFR expression levels, we treated A549-Plvx and A549-CD38 cells with NMN, respectively. We found that NMN treatment increased the protein level of DHFR in A549-CD38 cells, while it had little effect on that in A549-Plvx cells (Fig. 1E). The transcription level of *DHFR* slightly increased after NMN treatment in A549-CD38 cells (Fig. 1F), which suggested that NMN replenishment prevented DHFR degradation via increasing cellular NAD^+ level. Our previous studies showed that a NAD^+ decline by CD38 overexpression lead to the oxidative degradation of 15-PGDH (19). Therefore, these results indicated that CD38 overexpression may also cause the oxidative degradation of DHFR.

The oxidative degradation of DHFR is dependent on the proteasome pathways

To further confirm the oxidative degradation of DHFR, we treated A549 cells with different concentrations of hydrogen peroxide (H_2O_2) for 12 h, and found that the protein level of DHFR decreased gradually with the increase of H_2O_2 concentrations (Fig. 2A), while its transcription levels were unchanged (Fig. 2B).

Moreover, pretreatment with N-acetylcysteine (NAc) for 6 h prior to H_2O_2 treatment mitigated ROS-induced DHFR degradation (Fig. 2C), confirming the oxidative degradation of DHFR. MG132, a classical proteasome inhibitor, was used to pretreat A549 cells for 4 h before H_2O_2 treatment in order to determine whether DHFR degradation was proteasome-dependent. Indeed, ROS-induced DHFR degradation was inhibited by MG132 (Fig. 2D). However, bafilomycin A1 (Baf-A1), a known inhibitor of autophagy, had little effect on the ROS-induced DHFR degradation (Fig. 2E), suggesting that the oxidative degradation of DHFR was mainly dependent on the proteasome degradation pathway rather than the autophagy pathway.

ROS-caused sulfonation of cysteine7 in DHFR leads to its degradation

Human DHFR protein consists of eight β-sheets, constituting the rigid structure of protein molecule, and four α-helices, forming the binding sites of the substrate and coenzyme, and free loop structures, connecting β-sheets and α-helices (25–27). DHFR from different species shares high structural similarity (28). There is only one cysteine residue in DHFR at position 7 (Cys7) and DHFR contains no disulfide bonds (29). To figure out whether cysteine oxidation of DHFR leaded to its degradation, we established a stable cell line in which DHFR was overexpressed in A549 cells (A549-DHFR) (Fig. S1A and S1B). We found that the level of sulfonation on Cys7 in DHFR in cells treated with MG132 and H_2O_2 was about 4.5 times higher than that in the untreated cells by immunoprecipitation followed by LC-MS/MS analysis, as confirmed by the MS/MS spectrum of the sulfonated peptide (Fig. 3A). These results indicated that Cys7

located in β-sheet A was susceptible to oxidative stress, which may cause a change in its conformation and lead to its degradation.

To further confirm whether Cys7 oxidation caused its degradation, we carried out site-directed mutagenesis of Cys7, we constructed cell lines in which Cys7 was mutated to alanine (A549-DHFR-C7A) or mutated to aspartic acid (A549-DHFR-C7D) to eliminate Cys7 oxidation or to mimic the sulfonation of Cys7, respectively. Interestingly, only the Flag-tagged DHFR-C7A protein was detected while the Flag-tagged DHFR-C7D protein was barely detectible (Fig. 3B), which proved that sulfonation of Cys7 in DHFR caused its oxidative degradation. Moreover, MG132 treatment indeed significantly increased the level of Flag-tagged DHFR-C7D protein (Fig. 3C), which further confirmed that the oxidative degradation was proteasome-dependent.

CD38 high expression increases ferroptosis susceptibility via DHFR reduction

Considering that DHFR inhibits ferroptosis by catalyzing the reduction of BH_2 to the lipid peroxide reducer BH_4, we compared the susceptibility of A549-Plvx and A549-CD38 cells to ferroptosis inducers. Erastin and RSL3 are classic ferroptosis inducers that induce ferroptosis by inhibiting the System X_C^- and GPX4, respectively (30, 31). The survival of A549-CD38 cells was significantly lower than that of A549-Plvx cells when they were treated with Erastin or RSL3, suggesting that high expression of CD38 increased the susceptibility to ferroptosis (Fig. 4A and B).

We have found that NMN treatment prevented the oxidative degradation of DHFR in A549-CD38 cells (Fig. 1E). Therefore, we further examined the effect of NMN on ferroptosis susceptibility. Indeed, the ferroptosis induced by Erastin or RSL3 could be significantly alleviated by NMN in A549-CD38 cells according to the results of survival rate (Fig. 4C and D), suggesting that NMN suppressed the oxidative degradation of DHFR to decrease cellular susceptibility to ferroptosis. To further confirm the pivotal role of DHFR degradation in increasing ferroptosis susceptibility in A549-CD38 cells, we treated A549 cells with methotrexate (MTX), a known inhibitor of DHFR (15), and showed that MTX treatment significantly increased ferroptosis susceptibility of A549 cells (Fig. 4E and F). Furthermore, we replenished DHFR in CD38-overexpression cells and showed that the survival rates were increased (Fig. S2A and S2B; Fig. 4G and H). These results demonstrated that replenishing NMN or DHFR rescued A549-CD38 cells from ferroptosis, thus further confirming that the oxidative degradation of DHFR was responsible for the increased ferroptosis susceptibility.

BMDMs from aged mice are more susceptible to ferroptosis than those from young mice

Systemic inflammation accompanied with the decline in immune functions are related to age, which is newly named “inflammaging” (32, 33). A recent report revealed that senescence associated secretory phenotype (SASP) upregulated CD38 expression levels in macrophages (5, 34). However, it is unknown whether immune cells such as macrophages in aged organisms also increase the susceptibility to

ferroptosis, which in turn leads to functional decline. Therefore, we took BMDMs as an example to further explore whether ferroptosis susceptibility is increased during aging due to high expression of CD38.

First, we performed western blotting and qPCR analysis of BMDMs from aged and young mice, the protein and mRNA levels of CD38 in BMDMs from aged mice were significantly higher than those from young mice, while DHFR was lower (Fig. 5A and 5B). However, the transcription level of *DHFR* was slightly increased (Fig. 5C), which was consistent with the results of A549-CD38 cells. Therefore, we speculated that the decrease of DHFR in BMDMs from aged mice was likely resulted from oxidative degradation due to the high expression of CD38.

As expected, BMDMs from aged mice were more susceptible to ferroptosis (Fig. 5D and E). Iron chelator deferoxamine (DFO) and lipid peroxide reducers ferrostatin-1 (Fer-1), the classic ferroptosis inhibitors, alleviated ferroptosis induced by Erastin or RSL3, so was NMN (Fig. 5F and G), which was also consistent with the results of A549-CD38 cells. Therefore, we proposed that the elevated CD38 expression in BMDMs from aged mice also led to the oxidative degradation of DHFR, and rendered cells more susceptible to ferroptosis. More importantly, NMN supplementation reduced the susceptibility to ferroptosis in BMDMs in aged mice.

Discussion

It has been well documented that CD38 was upregulated in organs and macrophages in aged mice, which drives down the cellular NAD^+ level leading to age-associated organ malfunctions (4, 5, 7). Our previous studies have demonstrated that high expression of CD38 increases oxidative stress and downregulates proteins involved in glycolysis, DNA repair, and antioxidant (35). Importantly, we have revealed that CD38-mediated NAD^+ decline triggered oxidative degradation of 15-PGDH via protein sulfonation that drives cells to undergo EMT (19). However, it is not clear whether sulfonation-induced degradation can be applied into degradation of other proteins. The first aim in the present study was to examine DHFR downregulation revealed in our proteomic analysis. Using a cell model in which CD38 overexpression decreased the NAD^+ levels, we demonstrated that NAD^+ decline induced oxidative degradation of DHFR. We further revealed that ROS-induced sulfonation of Cys7 in DHFR triggered its degradation, which was proteasome dependent. Mutation of Cys7 to alanine (C7A) prevented DHFR degradation while mutation of Cys7 to aspartic acid (C7D) destabilized DHFR protein. Moreover, NMN replenishment reduced DHFR degradation. We also demonstrated that the oxidative degradation of DHFR, a known ferroptosis suppressor, increased the susceptibility to ferroptosis. Collectively, we showed that NAD^+ decline caused by CD38 high expression increased cellular susceptibility to ferroptosis via DHFR oxidative degradation, which was reverted by NMN supplementation.

To reveal the physiological relevance of the present finding, we isolated bone marrow monocytes from young and aged mice and induced them into BMDMs to verify the findings from A549-CD38 cells. Consistent with the results of A549-CD38 cells, BMDMs from aged mice were more susceptible to ferroptosis with the higher levels of CD38 and the lower levels of DHFR as compared with those from

young mice. NMN also decreased the ferroptosis susceptibility of BMDMs from aged mice. Aging is a multifactorial, inevitable process characterized as a gradual and progressive functional decline of physiological functions (36), imbalance of pro and antioxidants (37), ferrous ion retention, increased oxidative stress, and elevated inflammatory response (17, 38, 39). Aging also increases the risk of various disease, such as neurological disorders, diabetes, cancers, and ARDs. Characterization of aging associated ferroptosis in mammalian tissues and organs is important for understanding aging process (40).

In conclusion, our results demonstrated that oxidative degradation via protein sulfonation can be applied into the downregulation of DHFR in CD38-overexpression cells, and CD38-mediated NAD^+ decline increased ferroptosis susceptibility via DHFR oxidative degradation. Consistently, BMDMs from aged mice were more susceptible to ferroptosis with higher expression of CD38 and lower expression of DHFR. These results proposed that CD38 upregulation in aging cells rendered these cells more susceptible to ferroptosis. On the other hand, NMN executes its anti-aging function by inhibiting ferroptosis in aging cells.

Materials And Methods

Cell culture

Human lung cancer cell line A549 (Male), mouse fibroblast cell line L929 (Male), and human embryonic kidney cell line 293T (Female) were obtained from the cell bank of the Chinese Academy of Sciences (Shanghai, China). A549 and L929 cells were grown in RPMI-1640 medium (Wisent, Montreal, QC) supplemented with 10% FBS (Wisent, Montreal, QC) and 1% penicillin/streptomycin (Wisent, Montreal, QC). And 293T cells were grown in Dulbecco's Modified Eagle's Medium (Wisent, Montreal, QC) supplemented with 10% FBS (Wisent, Montreal, QC) and 1% penicillin/streptomycin (Wisent, Montreal, QC).

Cell line construction

pLVX-CD38-IRES-ZsGreen1 plasmid was constructed previously, on which CD38 DNA sequence encoding 2–43 amino acids were deleted and a Flag tag was added at its C-terminus. Then the CD38 DNA sequence was obtained from the pLVX-CD38-IRES-ZsGreen1 plasmid and cloned into the pLVX-IRES-mCherry plasmid to construct the pLVX-CD38-IRES-mCherry plasmid for further use. Besides, the DHFR DNA sequence was obtained from A549 cell line and cloned into the pLVX-IRES-ZsGreen1 plasmid hereinafter called pLVX-DHFR-IRES-ZsGreen1 plasmid.

293T cell lines were transfected with target plasmids together with helper plasmids for lentivirus packaging. Then A549 cells were infected with lentivirus and sorted by the BD FACSAria II Flow Cytometer (BD Biosciences, NJ, USA) to construct overexpression cell lines.

Cellular reactive oxygen species (ROS) measurement

The cellular ROS levels were determined by CellROX Deep Red Reagent (Invitrogen, NY, USA). Briefly, CellROX Deep Red reagent was applied to cells in complete medium and incubated for 30 min at 37°C. Then cells were washed with phosphate buffer (PH 7.2–7.6) 3 times, and then analyzed the mean fluorescence intensity at 665 nm by the BD FACSAria II Flow Cytometer (BD Biosciences, NJ, USA).

Western blotting

Cells were lysed in RIPA lysis buffer (Bryotime, Shanghai, China) supplemented with 1× protease inhibitor cocktail (Thermo-Pierce Biotechnology, Rockford, IL) and sonicated on ice. The protein concentration was determined by the BCA protein concentration assay kit (Bryotime, Shanghai, China) and equal amounts of proteins were separated by gel electrophoresis, and then electroblotted to the polyvinylidene difluoride (PVDF) membrane, blocked with 5% non-fat milk, incubated with the primary antibody and the secondary antibody sequentially. Finally, target proteins were detected using ECL reagent (Bio-Rad, CA, USA) and photographed by ChemiDoc™ XRS + SYSTEM (Bio-Rad, CA, USA). Primary antibodies for β-Actin (ABclonal, Woburn, MA), DHFR (Abcam, Cambridge, UK), CD38-human, CD38-mouse, Flag (Cell Signaling Technology, Danvers, MA), and secondary anti-rabbit HRP-IgG antibodies (Cell Signaling Technology, Danvers, MA) were used for detecting target proteins.

RNA isolation and real-time quantitative polymerase chain reaction analysis (qPCR)

Total RNA was extracted by TRNzol Universal Total RNA Extraction Reagent (TIANGEN, Beijing, China), which was then reverse transcribed into cDNA using reverse transcriptase (CWBIO, Beijing, China). SYBR green reaction mixture (CWBIO, Beijing, China) was used to perform qPCR with the Roche LightCycler 96 System (Roche, Basel, Switzerland). And ACTB was used as an internal control. All samples were performed in triplicate and the data were analyzed by Student's t-test. Primers used in qPCR were listed in Table S1.

Survival rate measurement

Cell counting kit-8 (CCK-8) was used to determine the survival rate by measuring the absorbance at 450 nm (A_{450}). Briefly, an equal number of cells were seeded into 96-well plates beforehand and then were treated under different conditions. After that, cells were washed with PBS and complete medium supplemented with 10% CCK-8 reagent (APExBIO, Boston, MA) was added to each well including the blank well (Blank control group). Then the plates were incubated in the cell incubator for about 2 h for further measuring A_{450}. And the survival rate was calculated according to the formula survival rate = (A_{450} Treatment group - A_{450} Blank control group) / (A_{450} Control group - A_{450} Blank control group)

Immunoprecipitation

For identifying the oxidative modification of DHFR, equal amounts of proteins from untreated, and 1 mM H_2O_2 + MG132 -treated A549-DHFR cell lines were incubated with Anti-Flag Affinity Gel (Bimake, Houston, TX) in 4°C on the rotator for about 6 h. After washing beads five times, 200 μL 0.1M Glycine HCl (PH = 3)

were applied to the beads and then rotated at a low speed for 5 ~ 10 min in order to elute the enriched DHFR-Flag protein. After that, the PH of supernatant was adjusted to around 7.4 and then added with 5× non-reducing SDS-PAGE loading buffer (CWBIO, Beijing, China) followed by in-gel digestion without reduction and heating and LC-MS/MS analysis.

In-gel digestion followed by LC-MS/MS analysis

Protein samples were separated by SDS-PAGE electrophoresis and target protein bands were excised, and then alkylated by incubating with 25 mM chloroacetamide for 45 min in the dark at 55℃ followed by digesting using trypsin (Promega, Fitchburg, WI) for 14 h at 37℃. The peptides were extracted three times with 50% acetonitrile supplemented with 0.1% formic acid and then vacuum dried peptides were dissolved in 20 μl 0.1% (v/v) formic acid and analyzed by LC-MS/MS analysis.

For LC-MS/MS analysis, peptides were loaded in a trap column and then separated by the Thermo-Dionex Ultimate 3000 HPLC system (Thermo Fisher Scientific, Waltham, MA, USA), and detected by the Obitrap Fusion LUMOS Tribrid mass spectrometer (Thermo Fisher Scientific, Waltham, MA, USA). Identification of protein modification was performed by Proteome Discoverer 2.3 software using the label-free quantification method.

Metabolomics analysis

The metabolomics analysis was performed as previously mentioned (41). Briefly, cells were incubated with pre-chilled 80% methanol for 2 h at − 80℃ after washed with PBS three times. Then cells were scraped and centrifuged at 12,000 rpm for 20 min at 4℃. The supernatant was vacuum dried, redissolved in 80% methanol, and analyzed by the TSQ Quantiva™ Triple Quadrupole Mass Spectrometer (Thermo Fisher Scientific, Waltham, MA, USA) with Ultimate 3000 in positive and negative ion switching mode. And the identification and quantification of target metabolites were performed by the Q-Exactive Mass Spectrometer (Thermo Fisher Scientific, Waltham, MA, USA) and TraceFinder according to the retention time and molecular mass of metabolites.

Isolation and culture of bone-marrow derived macrophages (BMDMs)

Female C57BL/6J mice (8 wk or 88wk) were housed under specific pathogen-free conditions at Laboratory Animal Research Center, Tsinghua University. The mice were used in accordance with Tsinghua Institutional Animal Care and Use Committee guidelines for animal welfare. BMDMs were derived from bone marrow monocytes in the femurs of euthanized mice (Young: 8-week-old female mice; Aged: 88-week-old female mice). Briefly, the muscle and connective tissue around the femurs were removed. The isolated femurs were washed with 75% ethanol twice, followed by 3 washes with PBS supplemented with1% penicillin/streptomycin. The bone marrow was flushed using a syringe, filtered through a 70 μm filter, and centrifuged at 1,000 rpm for 10 min at 4℃. The cell pellet was suspended in BMDM culture medium (RPMI-1640 medium supplemented with 30% L929 medium supernatant, 10%

FBS, and 1% penicillin/streptomycin) and then plated in a 10-cm dish. After culturing for 7 days, more than 95% of cells were macrophages (5).

Statistical analysis

Results are expressed as the means ± SD for n independent experiments, as indicated in the figure legends. All statistical analysis was processed using GraphPad Prism (version 8.0) and Image Lab. Student's t-test was used to calculate the difference between two independent groups and one-way ANOVA was used to compare three or more independent groups. A *P* value of < 0.05 was considered as evidence of statistical significance (*$p < 0.05$; **$p < 0.01$; ***$p < 0.001$, **** $p < 0.0001$).

Abbreviations

NAD, nicotinamide adenine dinucleotide; DHFR, dihydrofolate reductase; ROS, reactive oxygen species; BMDMs, bone-marrow derived macrophages; NMN, nicotinamide mononucleotide; ARDs, age-related disorders; ADPR, adenosine diphosphate ribose; cADPR, cyclic adenosine diphosphate ribose; PUFAs, polyunsaturated fatty acids; System X_C^-, cysteine/glutamate antiporter; GPX4, phospholipid hydroperoxide glutathione peroxidase 4; BH_4, tetrahydrobiopterin CoQ_{10}, coenzyme Q10; 15-PGDH, 15-hydroxyprostaglandin dehydrogenase; EMT, epithelial-mesenchymal transition; BH_2, dihydrobiopterin; PVDF, polyvinylidene difluoride; qPCR, real-time quantitative polymerase chain reaction; NAMPT, nicotinamide phosphoribosyltransferase; H_2O_2, hydrogen peroxide; NAc, N-acetylcysteine; Baf-A1, bafilomycin A1; MTX, methotrexate; SASP, senescent associated secretory phenotype; DFO, deferoxamine; Fer-1, ferrostatin-1.

Declarations

ACKNOWLEDGMENTS

This study was supported by the Ministry of Science and Technology of the People's Republic of China (grant No. 2017YFA0505103 and No. 2020YFC2002705), and National Natural Science Foundation of China (grant No. 21877068 and No. 20211300114). We greatly appreciate the Facility for Protein Chemistry and Proteomics at Tsinghua University for sample analysis.

CONFLICT OF INTEREST

The authors declare no competing interests.

AUTHOR CONTRIBUTIONS

Y.M. performed all the experiments except those mentioned below. M.Y. and Y.C. helped with some of the mass spectrometry analysis. W.W. performed the metabolomics analysis. Y.M. and H.D. designed the experiments. Q.W., C.L., Y.C. and H.D. supervised the project. Y.M. analysed the data and wrote the manuscript. Y.C. and H.D. revised the manuscript.

ETHICS DECLARATIONS

All animal experiments performed in this study were approved by the Tsinghua University Animal Care and Use Committee (TUACUC).

DATA AVAILABILITY

The experimental data in the current study are available from the corresponding author upon reasonable request. No applicable resources were generated during the current study.

References

1. Rajman L, Chwalek K, Sinclair DA. Therapeutic potential of NAD-boosting molecules: the in vivo evidence. Cell Metab. 2018;27(3):529-47.
2. Verdin E. NAD^+ in aging, metabolism, and neurodegeneration. Science. 2015;350(6265):1208-13.
3. Chini EN, Chini CC, Netto JME, de Oliveira GC, van Schooten W. The pharmacology of CD38/NADase: an emerging target in cancer and diseases of aging. Trends Pharmacol Sci. 2018;39(4):424-36.
4. Camacho-Pereira J, Tarragó MG, Chini CC, Nin V, Escande C, Warner GM, et al. CD38 dictates age-related NAD decline and mitochondrial dysfunction through an SIRT3-dependent mechanism. Cell Metab. 2016;23(6):1127-39.
5. Covarrubias AJ, Kale A, Perrone R, Lopez-Dominguez JA, Pisco AO, Kasler HG, et al. Senescent cells promote tissue NAD^+ decline during ageing via the activation of CD38+ macrophages. Nat Metab. 2020;2(11):1265-83.
6. Peclat TR, Thompson KL, Warner GM, Chini CC, Tarragó MG, Mazdeh DZ, et al. CD38 inhibitor 78c increases mice lifespan and healthspan in a model of chronological aging. Aging Cell. 2022;21(4):e13589.
7. Covarrubias AJ, Perrone R, Grozio A, Verdin E. NAD^+ metabolism and its roles in cellular processes during ageing. Nat Rev Mol Cell Biol. 2021;22(2):119-41.
8. Pencina KM, Lavu S, Dos Santos M, Beleva YM, Cheng M, Livingston D, et al. MIB-626, an Oral Formulation of a Microcrystalline Unique Polymorph of β-Nicotinamide Mononucleotide, Increases Circulating Nicotinamide Adenine Dinucleotide and its Metabolome in Middle-aged and Older Adults. The Journals of Gerontology Series A. 2022.
9. Dixon SJ, Lemberg KM, Lamprecht MR, Skouta R, Zaitsev EM, Gleason CE, et al. Ferroptosis: an iron-dependent form of nonapoptotic cell death. Cell. 2012;149(5):1060-72.
10. Li J, Cao F, Yin H-l, Huang Z-j, Lin Z-t, Mao N, et al. Ferroptosis: past, present and future. Cell Death Dis. 2020;11(2):1-13.
11. Feng H, Stockwell BR. Unsolved mysteries: How does lipid peroxidation cause ferroptosis? PLoS Biol. 2018;16(5):e2006203.

12. Rouzer CA, Marnett LJ. Mechanism of free radical oxygenation of polyunsaturated fatty acids by cyclooxygenases. Chem Rev. 2003;103(6):2239-304.
13. Cao JY, Dixon SJ. Mechanisms of ferroptosis. Cell Mol Life Sci. 2016;73(11):2195-209.
14. Tang D, Kroemer G. Ferroptosis. Curr Biol. 2020;30(21):R1292-R7.
15. Soula M, Weber RA, Zilka O, Alwaseem H, La K, Yen F, et al. Metabolic determinants of cancer cell sensitivity to canonical ferroptosis inducers. Nat Chem Biol. 2020;16(12):1351-60.
16. Larrick JW, Larrick JW, Mendelsohn AR. Contribution of ferroptosis to aging and frailty. Rejuvenation Res. 2020;23(5):434-8.
17. Toyokuni S, Yanatori I, Kong Y, Zheng H, Motooka Y, Jiang L. Ferroptosis at the crossroads of infection, aging and cancer. Cancer Sci. 2020;111(8):2665-71.
18. Zhao T, Guo X, Sun Y. Iron Accumulation and Lipid Peroxidation in the Aging Retina: Implication of Ferroptosis in Age-Related Macular Degeneration. Aging Dis. 2021;12(2):529-51.
19. Wang W, Hu Y, Wang X, Wang Q, Deng H. ROS-mediated 15-hydroxyprostaglandin dehydrogenase degradation via cysteine oxidation promotes NAD^+-mediated epithelial-mesenchymal transition. Cell Chem Biol. 2018;25(3):255-61. e4.
20. Nehring H, Meierjohann S, Friedmann Angeli JP. Emerging aspects in the regulation of ferroptosis. Biochem Soc Trans. 2020;48(5):2253-9.
21. Zheng J, Conrad M. The metabolic underpinnings of ferroptosis. Cell Metab. 2020;32(6):920-37.
22. Imai S-i, Yoshino J. The importance of NAMPT/NAD/SIRT1 in the systemic regulation of metabolism and ageing. Diabetes Obes Metab. 2013;15(s3):26-33.
23. Lanska DJ. The discovery of niacin, biotin, and pantothenic acid. Ann Nutr Metab. 2012;61(3):246-53.
24. Yoshino J, Mills KF, Yoon MJ, Imai S-i. Nicotinamide mononucleotide, a key NAD^+ intermediate, treats the pathophysiology of diet-and age-induced diabetes in mice. Cell Metab. 2011;14(4):528-36.
25. Cody V, Schwalbe CH. Structural characteristics of antifolate dihydrofolate reductase enzyme interactions. Crystallogr Rev. 2006;12(4):301-33.
26. Davies JF, Delcamp TJ, Prendergast NJ, Ashford VA, Freisheim JH, Kraut J. Crystal structures of recombinant human dihydrofolate reductase complexed with folate and 5-deazafolate. Biochemistry. 1990;29(40):9467-79.
27. Lockyer J, Cook RG, Milstien S, Kaufman S, Woo S, Ledley FD. Structure and expression of human dihydropteridine reductase. Proc Natl Acad Sci U S A. 1987;84(10):3329-33.
28. Rao A, Tapale S. A study on dihydrofolate reductase and its inhibitors: A review. Int J of Pharm Sci Res. 2013;4(2535):2535-47.
29. Polshakov V. Dihydrofolate reductase: structural aspects of mechanisms of enzyme catalysis and inhibition. Russ Chem Bull. 2001;50(10):1733-51.
30. Dolma S, Lessnick SL, Hahn WC, Stockwell BR. Identification of genotype-selective antitumor agents using synthetic lethal chemical screening in engineered human tumor cells. Cancer Cell.

2003;3(3):285-96.
31. Yang WS, Kim KJ, Gaschler MM, Patel M, Shchepinov MS, Stockwell BR. Peroxidation of polyunsaturated fatty acids by lipoxygenases drives ferroptosis. Proc Natl Acad Sci U S A. 2016;113(34):E4966-E75.
32. Franceschi C, Garagnani P, Parini P, Giuliani C, Santoro A. Inflammaging: a new immune–metabolic viewpoint for age-related diseases. Nat Rev Endocrinol. 2018;14(10):576-90.
33. Zuo L, Prather ER, Stetskiv M, Garrison DE, Meade JR, Peace TI, et al. Inflammaging and oxidative stress in human diseases: from molecular mechanisms to novel treatments. Intl J of Mol Sci. 2019;20(18):4472.
34. Coppé J-P, Desprez P-Y, Krtolica A, Campisi J. The senescence-associated secretory phenotype: the dark side of tumor suppression. Ann Rev Pathol. 2010;5:99-118.
35. Hu Y, Wang H, Wang Q, Deng H. Overexpression of CD38 decreases cellular NAD levels and alters the expression of proteins involved in energy metabolism and antioxidant defense. J Proteome Res. 2014;13(2):786-95.
36. López-Otín C, Blasco MA, Partridge L, Serrano M, Kroemer G. The hallmarks of aging. Cell. 2013;153(6):1194-217.
37. Zuo L, Zhou T, Pannell B, Ziegler A, Best T. Biological and physiological role of reactive oxygen species–the good, the bad and the ugly. Acta Physiol (Oxf). 2015;214(3):329-48.
38. Mazhar M, Din AU, Ali H, Yang G, Ren W, Wang L, et al. Implication of ferroptosis in aging. Cell Death Discov. 2021;7(1):1-9.
39. Höhn A, Weber D, Jung T, Ott C, Hugo M, Kochlik B, et al. Happily (n)ever after: Aging in the context of oxidative stress, proteostasis loss and cellular senescence. Redox Biol. 2017;11:482-501.
40. Niccoli T, Partridge L. Ageing as a risk factor for disease. Curr Biol. 2012;22(17):R741-R52.
41. Xu J, Zhu S, Xu L, Liu X, Ding W, Wang Q, et al. CA9 silencing promotes mitochondrial biogenesis, increases putrescine toxicity and decreases cell motility to suppress ccRCC progression. Int J of Mol Sci. 2020;21(16):5939.

Figures

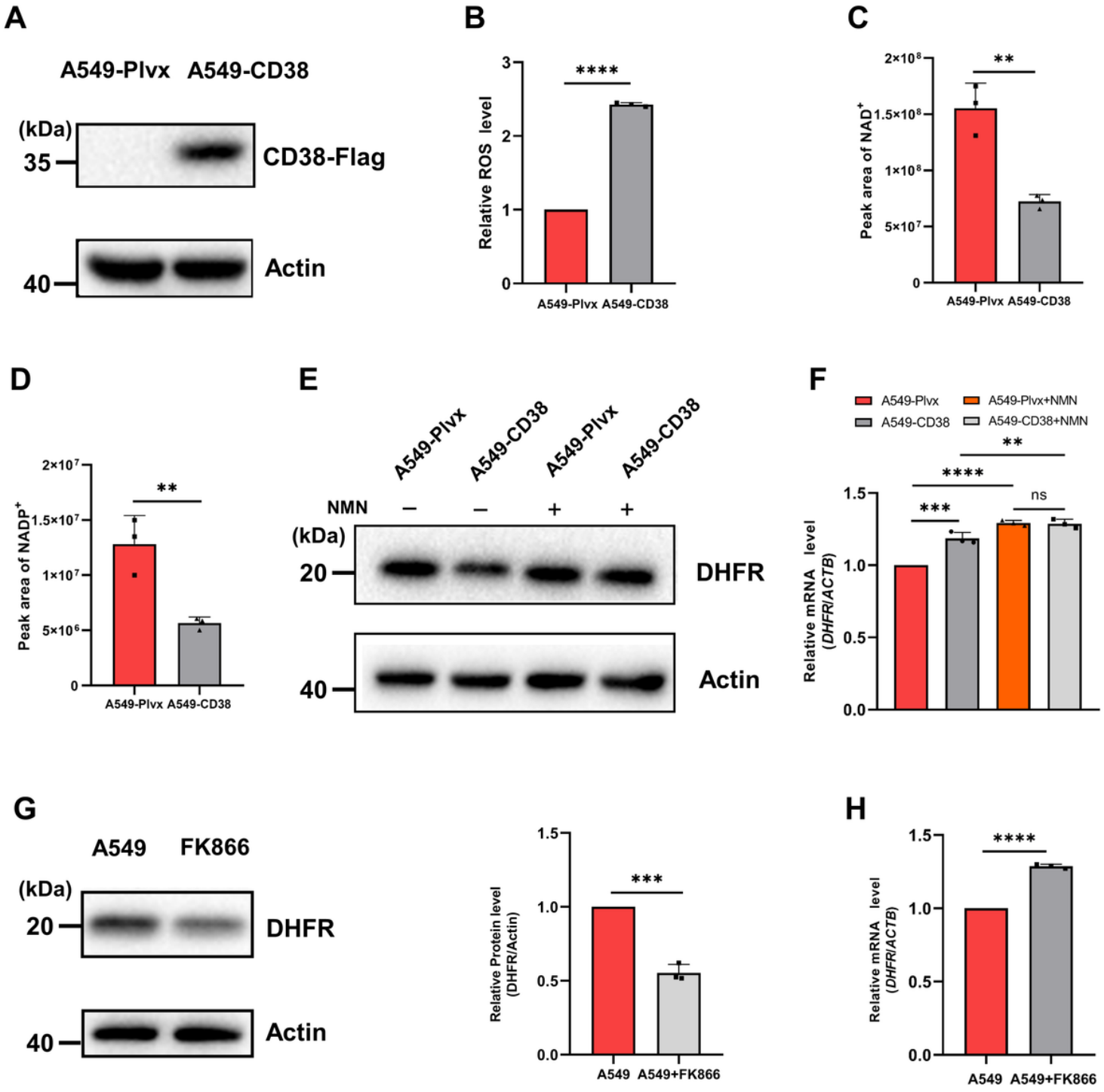

Figure 1

High expression of CD38 causes oxidative degradation of DHFR. A Western blot analysis confirmed CD38 overexpression in A549-CD38 cells compared with A549-Plvx cells. **B** Relative ROS levels in A549-Plvx and A549-CD38 cells. n=3. **C-D** NAD^+ and $NADP^+$ levels in A549-Plvx and A549-CD38 cells determined by peak areas from the metabolomics analysis. n=3. **E-F** Protein and mRNA expression levels of DHFR in A549-Plvx and A549-CD38 cells treated with or without 1 mM NMN. n=3. **G-H** Protein and mRNA expression levels of DHFR in untreated and 100 nM FK866-treated A549 cells. n=3. Data were shown as

mean ± SD and analyzed by Student's t-test or one-way ANOVA test. *p < 0.05, **p < 0.01, ***p < 0.001, ****p < 0.0001.

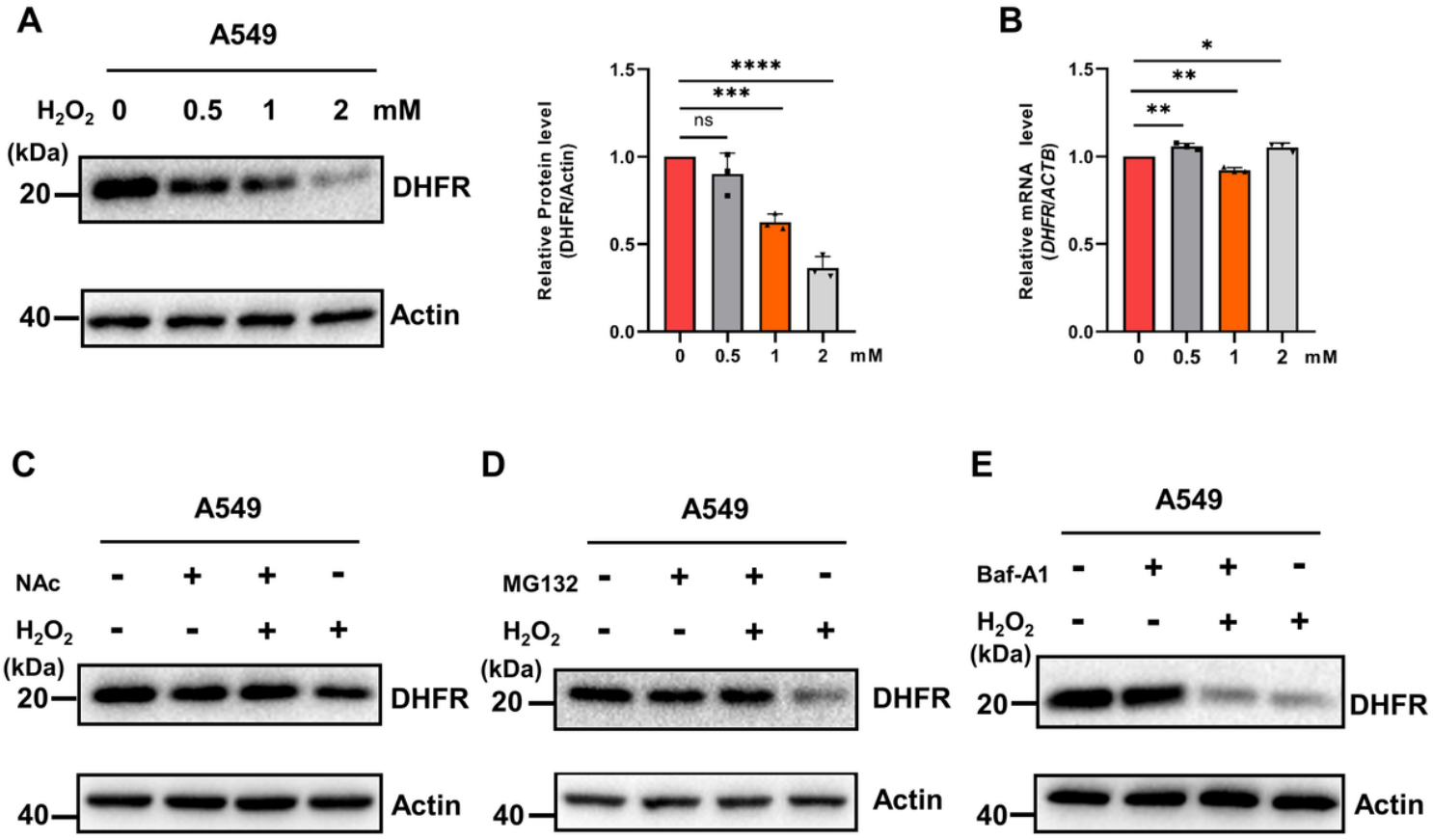

Figure 2

The oxidative degradation of DHFR is mediated by the proteasome pathway. A Western blot images of DHFR in A549 cells treated with different concentrations of H_2O_2 for 12 h. n-3. Data were shown as mean ± SD and analyzed by one-way ANOVA test. *p < 0.05, **p < 0.01, ***p < 0.001, ****p < 0.0001. **B** The mRNA expression level of DHFR in A549 cells treated with different concentrations of H_2O_2 for 12 h. n-3. Data were shown as mean ± SD and analyzed by one-way ANOVA test. *p < 0.05, **p < 0.01, ***p < 0.001, ****p < 0.0001. **C** Western blot images of DHFR in untreated and H_2O_2-treated A549 cells with or without prior treatment with 6 mM NAc for 6 h. **D** Western blot images of DHFR in untreated and H_2O_2-treated A549 cells with or without prior treatment with 10 μM MG132 for 4 h. **E** Western blot images of DHFR in untreated and H_2O_2-treated A549 cells with or without co-treatment with 100 nM Baf-A1.

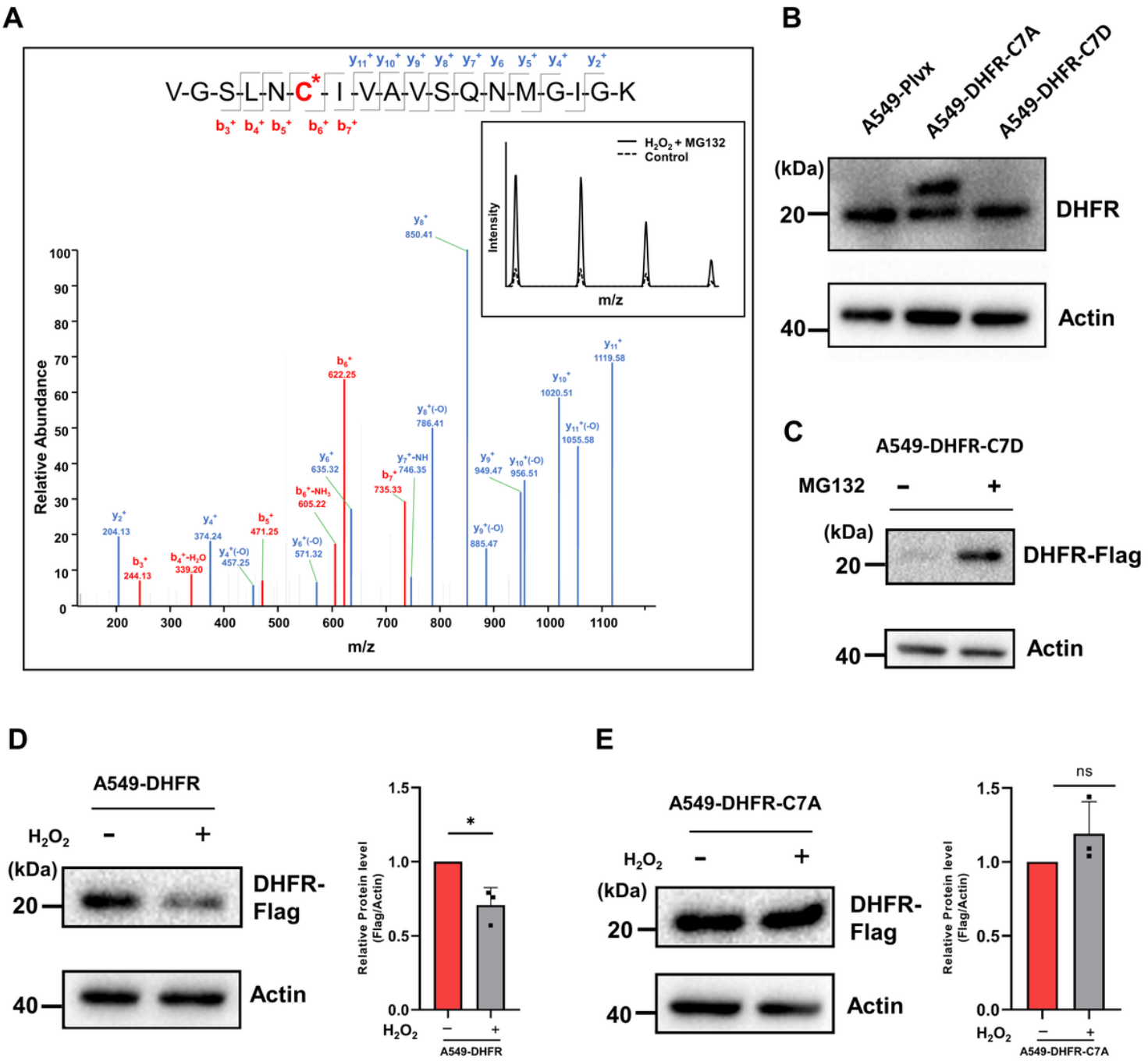

Figure 3

The sulfonation of Cys7 in DHFR induces its oxidative degradation. A Mass spectrometry spectrum of the peptide containing sulfonated Cys7 in DHFR, with the inset illustrating the ion intensity of the peptide from untreated and H_2O_2-MG132 co-treated cells. **B** Western blot images of the expression levels of DHFR and mutated DHFR proteins from A549-Plvx, A549-DHFR-C7A and A549-DHFR-C7D cells. **C** Western blot images of DHFR-C7D protein from untreated and MG132 treated cells. **D-E** Western blotting analysis of DHFR protein form untreated and H_2O_2 treated A549-DHFR and A549-DHFR-C7A cells, respectively. n=3. Data were shown as mean ± SD and analyzed by Student's t-test. *p < 0.05, **p < 0.01, ***p < 0.001, ****p < 0.0001.

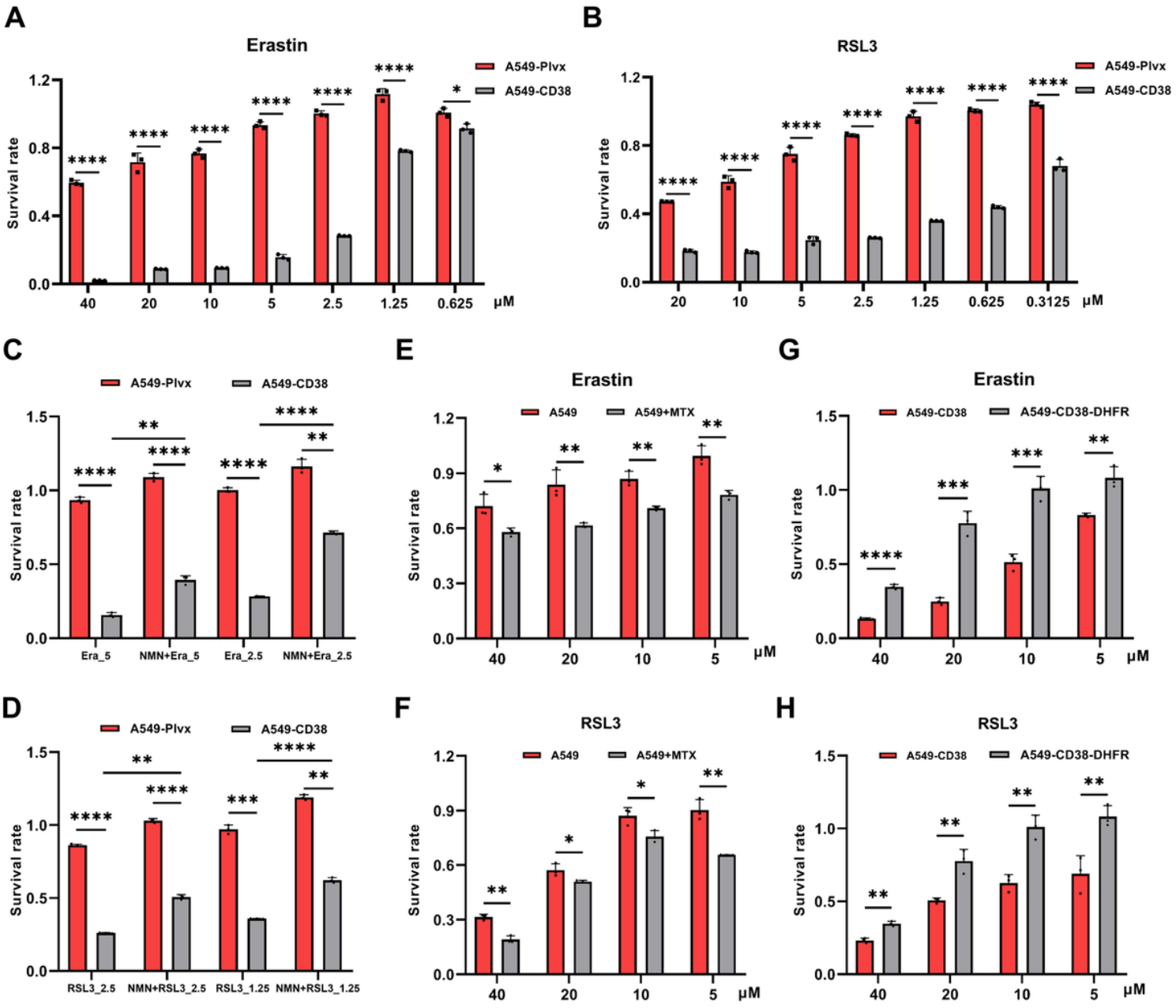

Figure 4

High expression of CD38 increases ferroptosis susceptibility. **A-B** The survival rate of A549-Plvx and A549-CD38 cells treated with different concentrations of Erastin (A) or RSL3 (B). n=3. **C-D** The survival rate of A549-Plvx and A549-CD38 cells under Erastin (5 μM, 2.5 μM or RSL3 (2.5 μM, 1.25 μM) treatment with or without 1 mM NMN. n=3. **E-F** The survival rate of A549 cells under Erastin or RSL3 treatment with or without 100 nM methotrexate (MTX). n=3. **G-H** The survival rate of A549-CD38 cells under Erastin or RSL3 treatment before or after replenishing DHFR. n=3. Data were shown as mean ± SD and analyzed by Student's t-test or one-way ANOVA test. *p < 0.05, **p < 0.01, ***p < 0.001, ****p < 0.0001.

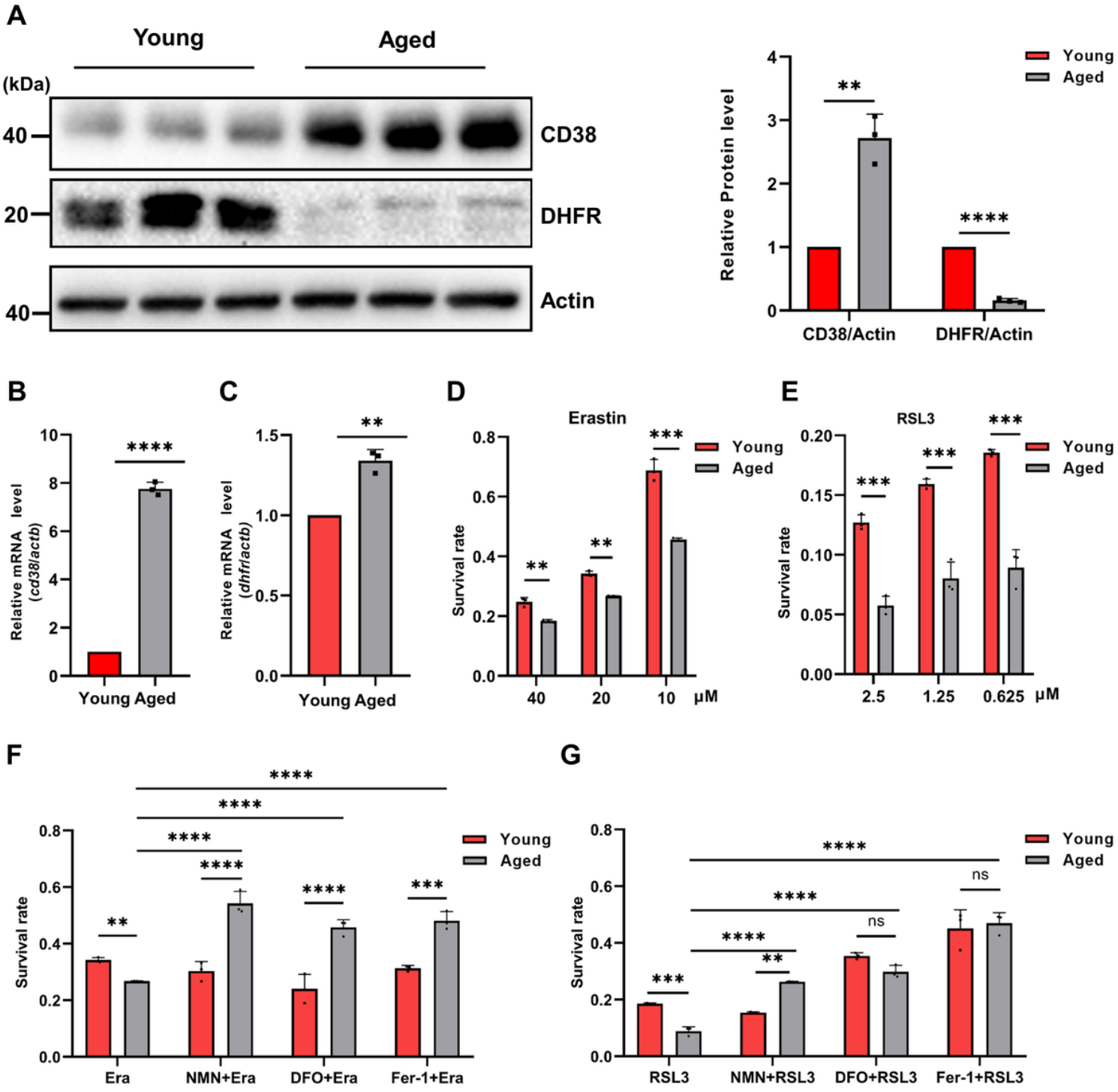

Figure 5

BMDMs from aged mice are more susceptible to ferroptosis. A Western blot analysis of CD38 and DHFR in BMDMs from young and aged mice, respectively. **B-C** The mRNA expression level of *CD38* and *DHFR* in BMDMs from young and aged mice, respectively. **D-E** The survival rate of BMDMs from young and aged mice under Erastin (D) or RSL3 (E) treatment. **F** The survival rate of BMDMs from young and aged mice under Erastin (20 μM), NMN (1 mM) + Erastin (20 μM), DFO (50 μM) + Erastin (20 μM), and Fer-1 (1 μM) + Erastin (20 μM) treatment. **G** The survival rate of BMDMs from young and aged mice under RSL3 (0.625 μM), NMN (1 mM) + RSL3 (0.625 μM), DFO (50 μM) + RSL3 (0.625 μM), and Fer-1 (1 μM) + RSL3 (0.625

μM). Data were shown as mean ± SD and analyzed by Student's t-test or one-way ANOVA. *p < 0.05, **p < 0.01, ***p < 0.001, ****p < 0.0001.

Supplementary Files

This is a list of supplementary files associated with this preprint. Click to download.

- Originalwesternblots.pdf
- SupplementaryInformation.pdf